Broadband Wide-Angle VElocity Selector (BWAVES) neutron spectrometer designed for the SNS Second Target Station

Eugene Mamontov[1,*], *Heloisa* N. Bordallo[2], *Olivier* Delaire[3], *Jonathan* Nickels[4], *Judith* Peters[5], *Gerald J.* Schneider[6], *Jeremy C.* Smith[7], and *Alexei P.* Sokolov[8]

[1]Second Target Station Project, Oak Ridge National Laboratory, Oak Ridge, Tennessee 37831, USA
[2]Niels Bohr Institute, University of Copenhagen, Copenhagen, Denmark
[3]Department of Mechanical Engineering and Materials Science, Department of Physics, and Department of Chemistry, Duke University, Durham, North Carolina 27708 USA
[4]Department of Chemical and Environmental Engineering, University of Cincinnati, Ohio 45221, USA
[5]Univ. Grenoble Alpes, CNRS, LiPhy and Institut Universitaire de France, and Institut Laue-Langevin, Grenoble, France
[6] Department of Chemistry and Department of Physics & Astronomy, Louisiana State University, Baton Rouge, Louisiana 70803, USA
[7]UT/ORNL Center for Molecular Biophysics, Oak Ridge National Laboratory, Oak Ridge, Tennessee 37831, USA and Department of Biochemistry & Cellular and Molecular Biology, University of Tennessee, Knoxville, Tennessee 37996, USA
[8]Chemical Sciences Division, Oak Ridge National Laboratory, Oak Ridge, Tennessee 37831, USA and Department of Chemistry, University of Tennessee, Knoxville, Tennessee 37996, USA

Abstract. A recently proposed wide-angle velocity selector (WAVES) device for choosing the velocity of detected neutrons after they have been scattered by the sample paves the way for inverted geometry neutron spectrometers with continuously adjustable final neutron wavelength. BWAVES broadband inverted geometry spectrometer proposed for the Second Target Station at the Spallation Neutron Source at Oak Ridge National Laboratory is designed using WAVES to simultaneously probe dynamic processes spanning 4.5 decades in time (energy transfer). This makes BWAVES a uniquely flexible instrument which can be viewed as either a quasielasitc neutron scattering (QENS) spectrometer with a practically unlimited (overlapping with the vibrational excitations) range of energy transfers, or a broadband inelastic vibrational neutron spectrometer with QENS capabilities, including a range of accessible momentum transfer (Q) and a sufficiently high energy resolution at the elastic line. The new capabilities offered by BWAVES will expand the application of neutron scattering in ways not possible with existing neutron spectrometers.

1 Introduction

Inelastic neutron scattering (INS) is a powerful technique for probing atomic and molecular-level dynamics in condensed matter. The type of a neutron spectrometer (e.g., direct vs. inverted geometry) largely defines the scientific areas that the instrument is best capable of addressing. Inverted geometry neutron spectrometers measure neutrons scattered by the sample with a certain fixed "final" momentum and energy, $\mathbf{k}_f$ and E_f. From a range of the momenta and energies in the neutron beam incident on the sample, the "initial" momentum and energy, $\mathbf{k}_i$ and E_i, are found for a particular detected neutron using its time-of-flight TOF from the source to the sample to the detector. This determines the momentum and energy transfer, $Q = |\mathbf{Q}| = |\mathbf{k}_i - \mathbf{k}_f|$ and $E = E_i - E_f$, for each detected neutron scattered by the sample. A sum of all scattering events gives the scattering intensity, I(Q,E) that is proportional to the dynamic structure factor, S(Q,E), $E=\hbar\omega$, which can be interpreted as a double Fourier transformation of the particle's van Hove correlation function, G(r,t) which is classically the probability of finding a particle at position r after time t. INS thus uniquely provides simultaneous information on both the geometries of motions via the Q dependence and the time dependence via E. Further, the simple relation between S(Q,E) and G(r,t) illustrates that INS is a uniquely direct probe of atomic motion, requiring no extra knowledge of electronic, optical, or other properties for its interpretation.

Scattering of neutrons by a sample is comprised of coherent and incoherent parts, and measurements are usually designed to minimize the undesirable contribution from either signal. Inverted geometry neutron spectrometers tend to be utilized for measurements of predominantly incoherently scattering, usually hydrogen-bearing, samples. This is largely because the two prominent classes of such spectrometers, molecular vibrational and backscattering, efficiently utilize the main advantages of the inverted geometry: access to a broad range of energy transfers, even at low temperatures, and a high energy resolution at the elastic line. However, even the recently deployed high energy-resolution backscattering spectrometers [1-4], which excel in probing stochastic

* Corresponding author: mamontove@ornl.gov

dynamics that give rise to quasielastic neutron scattering (QENS), suffer from a limited range of available energy transfers. At the same time, broadband molecular vibrational spectrometers [5,6] lack the energy resolution and Q-coverage to probe QENS-type signal due to stochastic dynamics.

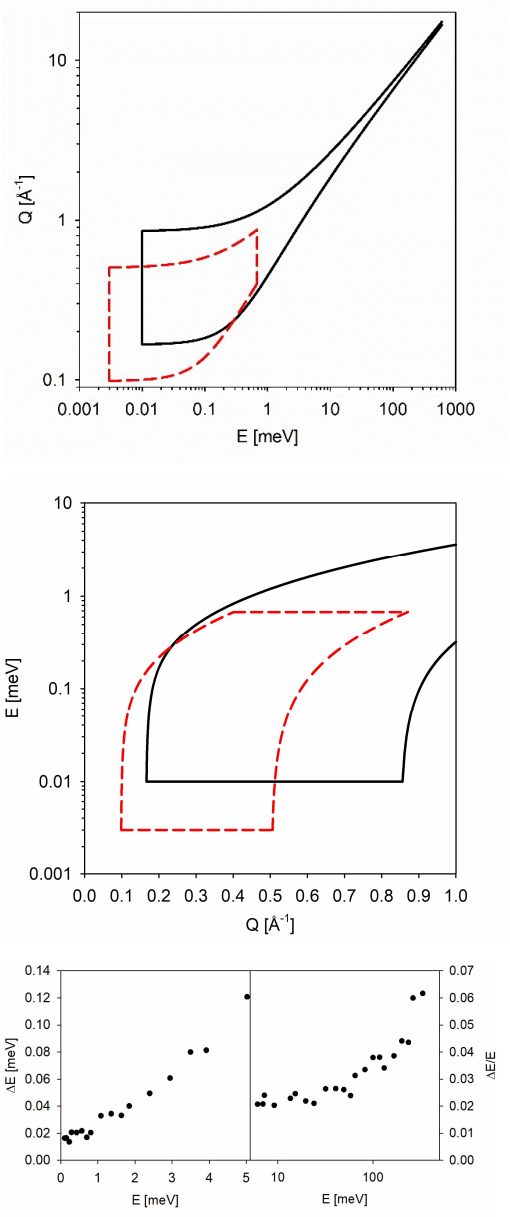

Fig. 1. Top panel: solid lines: the (E,Q) space coverage provided by the BWAVES spectrometer using the default λ_f = 14.50 Å in the standard operation mode. Also presented (dashed lines) is an example of the BWAVES "booster" mode with λ_f = 24.50 Å chosen for illustration. Middle panel: zoomed-in and truncated data from the top panel replotted as a function of Q. Bottom panel: the simulated energy resolution of BWAVES. Absolute energy resolution, ΔE (full width at half-maximum), up to 5 meV (left) and relative energy resolution, ΔE/E above 5 meV (right).

To address these shortcomings, a proposal has been recently approved to construct an inverted geometry spectrometer at the Spallation Neutron Source (SNS) Second Target Station (STS). Named BWAVES, which is an acronym for broad-band wide-angle velocity selector spectrometer, the spectrometer utilizes a novel wide-angle velocity selector (WAVES) device [7] to choose the velocity of neutrons after they have been scattered by the sample. BWAVES employs several novel technical solutions (besides the use of WAVES), as described in detail elsewhere [8], to become:

(1) a spectrometer with an unmatched dynamic range covering energy transfers from below 0.010 meV to above 500 meV.

(2) the only inverted geometry spectrometer currently proposed for SNS STS, well suited to map relaxational excitations that gradually emerge as a function of temperature, thereby efficiently deciphering complex dynamic landscapes.

(3) a spectrometer with a small beam size (5 mm by 5 mm), thus enabling studies of small samples and facilitating the use of advanced sample environment equipment.

(4) an open-tabletop sample geometry instrument, providing easy access to the sample position for application of external stimuli and multimodal experimentation, which includes default optical access to the sample.

(5) the gateway (oftentimes, the one-stop) spectrometer for neutron scattering studies of dynamics in materials, which is analogous to the role played by a general-purpose small-angle or broad-angle neutron diffractometer for structural studies.

Fig. 2. A photo of a prototype WAVES device for selection of the final wavelength of the neutrons scattered at the sample position.

While each of these features is prominent on its own, the broadband character of BWAVES spectra is perhaps of utmost importance. The remarkable coverage of (E,Q) space, which at BWAVES is achieved within a single neutron frame (before the next proton pulse hits the target), is illustrated in Fig. 1, together with the energy resolution simulated using McStas [9,10] and MCViNE [11,12] packages. The widest dynamic range can be available at a non-constant Q.

A WAVES rotor is designed and built with curved blades of a shape described in polar coordinates as r = Aφ, A = v_f/(360°f), where v_f is the intended velocity of the neutrons transmitted by the rotor, and f is the rotation frequency. A photo of a prototype WAVES rotor is presented in Fig. 2. The WAVES resolution (full width

at half-maximum) can be evaluated [7] as $\Delta E_f = 2E_f(360°A/n_b(R_{max} - R_{min})) = 2E_f((v_f/f)/n_b(R_{max} - R_{min}))$, where n_b is the number of blades with an internal and an external radius of R_{min} and R_{max} and E_f is the energy of the neutrons transmitted by the rotor. Thus, when designing blades for a WAVES rotor, the maximum rotational frequency is chosen for the target v_f to improve the energy resolution. As a consequence, for a given WAVES rotor with a blade shape of $r = A\varphi$, a longer transmission wavelength, resulting in a finer energy resolution, can be readily chosen by lowering the rotation frequency and, therefore, the transmitted neutron velocity, because for a neutron to be transmitted, the ratio of (v_f/f) must remain constant. In contrast, a higher transmission neutron velocity (a shorter λ_f) cannot be selected readily, because this would require increasing the rotation frequency, which is already chosen to be as high as is technically feasible to ensure the best possible energy resolution in the standard operation mode. A freely selectable, in a continuous fashion, longer transmission wavelength results in finer energy resolution, and such an operation regime is thus dubbed a "booster" mode. An example of the BWAVES coverage in the (E,Q) space in the "booster" mode using an arbitrarily chosen $\lambda_f = 24.50$ Å is also presented in Fig. 1.

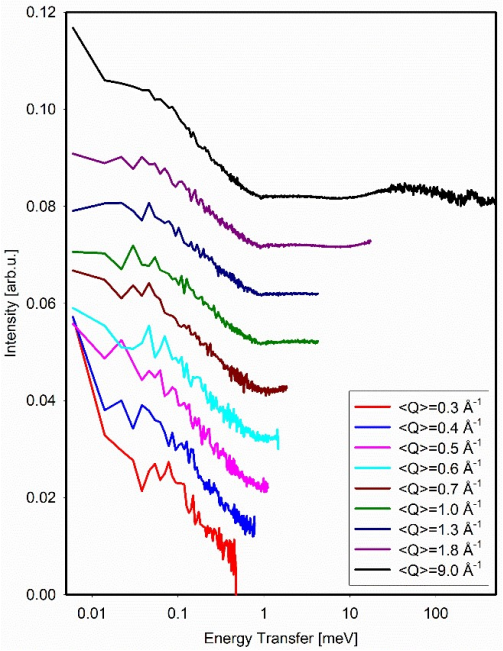

Fig. 3. HIV-1 protease at 120 K, measured at BWAVES using the default $\lambda_f = 14.50$ Å for 5 hours (virtually). The nine average <Q> values refer to the Q-bins of 0.25-0.35 Å^{-1}, 0.35-0.45 Å^{-1}, 0.45-0.55 Å^{-1}, 0.55-0.65 Å^{-1}, 0.65-0.75 Å^{-1}, 0.75-1.25 Å^{-1}, 0.75-1.85 Å^{-1}, 0.75-2.85 Å^{-1}, and 0.15-17.85 Å^{-1}.

Fig. 3 illustrates the output of a virtual BWAVES experiment to measure dynamics of HIV-1 protease. evaluated using McStas [9,10] and MCViNE [11,12] packages. In agreement with the data presented in Fig. 1, as the Q increases, plotting continuous broadband spectra requires the use of progressively broader Q-bins. The maximum possible dynamic range is attained for the data integrated over all scattering angles, similar to molecular vibrational spectrometers [5,6]. The dynamic scattering kernel, S(Q,E) for this system was mainly developed in the course of carrying out modelling for the recently published study revealing dynamical softening in the HIV-1 protease upon binding of an inhibitor darunavir [13], a finding of particular importance in determining the physical factors leading to inhibition of this critical drug target. The virtual neutron scattering experiment at BWAVES was performed using a D_2O-hydrated protein powder sample of HIV-1 protease, loaded in a cylindrical sample holder, 5 mm in height and 5 mm in diameter, with the packing density to give the total incoherent scattering cross-section for the sample of 0.2 cm^{-1} (that is, a 10% incoherent scatterer with the BWAVES design sample geometry). The higher-energy data in Fig. 3 show vibrational spectrum, with the C-H stretch modes visible near 300 meV. The lower-energy part of the spectrum exhibits what appears to be two components, with the positions independent of Q, indicative of the localized relaxational dynamics. It should be noted that development of yet another QENS component, due to the water solvent-driven protein dynamics, could be expected at higher measurement temperatures in this system.

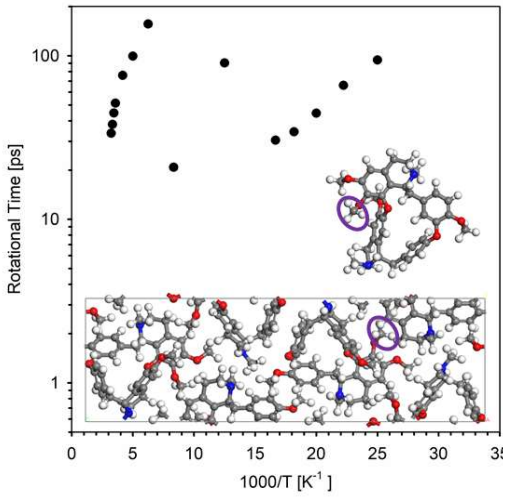

Fig. 4. Arrhenius plot of the measured relaxation times (symbols) for the methyl group rotation in a molecular drug tetrandrine (the data points are adapted from [14]). Insets: molecular structure (top) and crystal structure (bottom) of tetrandrine. The methyl group with the lowest rotational barrier, giving rise to the low-temperature data points, are encircled by an oval. The other methyl groups have higher rotational barriers and give rise to the high-temperature data points.

Another illustration of the advantage of an inverted geometry spectrometer with a broad dynamic range is provided by Fig. 4. Our recent efforts to characterize the dynamics of methyl groups in an antiviral molecular drug tetrandrine [14] were complicated by the fact that there are six methyl groups per tetrandrine molecule (Fig. 4). A series of the temperature dependent QENS measurements carried out

at the SNS backscattering spectrometer BASIS (with a ±0.1 meV range of energy transfer) gives a non-monotonic temperature dependence for the methyl rotational jump time (Fig. 4). The reason for this is that, above 60 K, the quasielastic signal from the tetrandrine methyl group with the lowest rotational barrier, which first emerges on warming up from the baseline temperature, becomes too broad for BASIS to measure. However, the other methyl group rotational signals gradually enter (and eventually exit) the spectrometer's accessible range of energy transfers, thereby giving rise to the apparent non-monotonic temperature dependence of the measured rotational jump time. In contrast, measurements at BWAVES, with its wide range of accessible energy transfers, carried out while gradually raising the temperature from the baseline, will show the emergence of the methyl group dynamics with increasing rotational barriers one by one together with the simultaneous shift to the high energy (but not disappearance) of the methyl group dynamics with the lower rotational barriers. Thus, the dynamics of all the methyl groups would be identified, revealing their activation energies, which will also be linked to the vibrational modes simultaneously measured from the INS part of the spectrum. This approach requires access to the full relevant dynamic range, even at low measurement temperatures, not being constrained by detailed balance limitations, which can be achieved with inverted, but not direct, geometry spectrometers. As the only inverted geometry spectrometer currently proposed for SNS STS, BWAVES will be uniquely suited to systematically map the relaxational excitations as they gradually emerge with increasing temperature.

The technical details of BWAVES and its components are thoroughly described elsewhere [8]. This paper concentrates on the relationship between the unusual characteristics of BWAVES and the science it is anticipated to enable.

2 Science enabled by BWAVES

2.1 Molecular dynamics in soft matter

Soft matter is a broad class of materials including, among others, liquids and polymers, colloids and foams, lipid assemblies, and biological systems. Soft materials are used in many current technologies with significant potential for breakthrough future applications. One of the major properties of soft matter is an enormous number of metastable states with only small differences in their free energies, of the order of kT. As a result, soft-matter systems fluctuate rapidly between these states, and such fluctuations and rearrangements define their unique properties. However, the enormous number of metastable states leads to a very high complexity of these materials, with a broad range of relaxation phenomena, dynamic heterogeneities, cooperativity, and ageing of non-equilibrium states. QENS and INS provide critical information on transitions between the metastable states as well as a broad range of collective and individual dynamics in soft matter systems, including liquids, lipid assemblies and polymers. QENS/INS also helps unravel detailed mechanisms of proton/ion transport and elucidate many other aspects of soft matter dynamics. As a typical example, a combination of separately measured scattering spectra from polymer systems is usually necessary for thorough

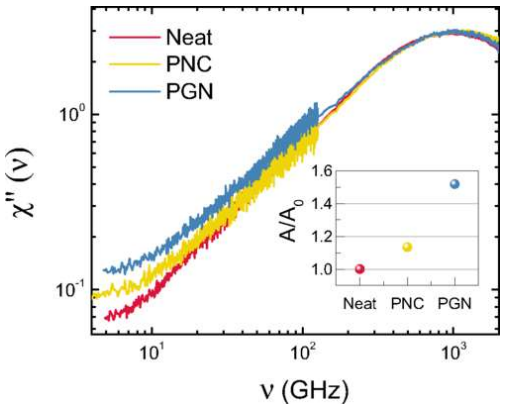

Fig. 5. Neutron scattering data presented as susceptibilities (T = 300 K, summed over all Q values, combined BASIS (SNS) and CNCS (SNS) measurements). The inset shows the normalized QENS area under the curve of a neat polymer vs. the polymer nanocomposite (PNC) and the polymer grafted to nanoparticles (PGN). Reprinted with permission from [15]. Copyright 2017 by the American Physical Society.

characterization of the polymer dynamics (Fig. 5, [15]), but unfortunately this relies on arbitrary matching of the data from different spectrometers summed over all Q values. In contrast, with its broad dynamic range

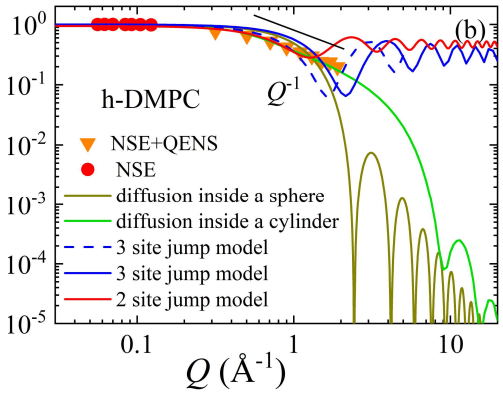

Fig. 6. Elastic incoherent structure factor for h-DMPC lipids obtained from NSE (SNS) and BASIS (SNS) studies. The data are modeled with motions within a sphere, a cylinder, and compared with three and two site jump models. Reprinted with permission from [18]. Copyright 2020 The Royal Society of Chemistry.

BWAVES will be an ideal instrument to enable unequivocal analysis of polymer dynamics, including the geometries of molecular motions via the Q dependence of the scattering signal over the broad energy range. BWAVES will be well suited for measurements of dynamics in complex polymer systems, e.g., as presented in recently published studies of bottlebrush polymers [16,17] that had to utilize several neutron spectrometers at different facilities.

In another example, liposomes are an excellent model system for studying non-covalent interactions in complex cell membranes. Neutron spectroscopic studies of liposomes will shed light on effects of drugs, investigate how viruses enter a cell membrane, and suggest how to harness the properties of cell membranes in technical applications, e.g., with embedded molecules for light harvesting. A recent study [18] combined data collected at the SNS neutron spin-echo (NSE) and BASIS spectrometers to cover a broad Q-range in the time range shorter than 5 ns. Fig. 6 shows the obtained elastic incoherent structure factor (EISF) representing

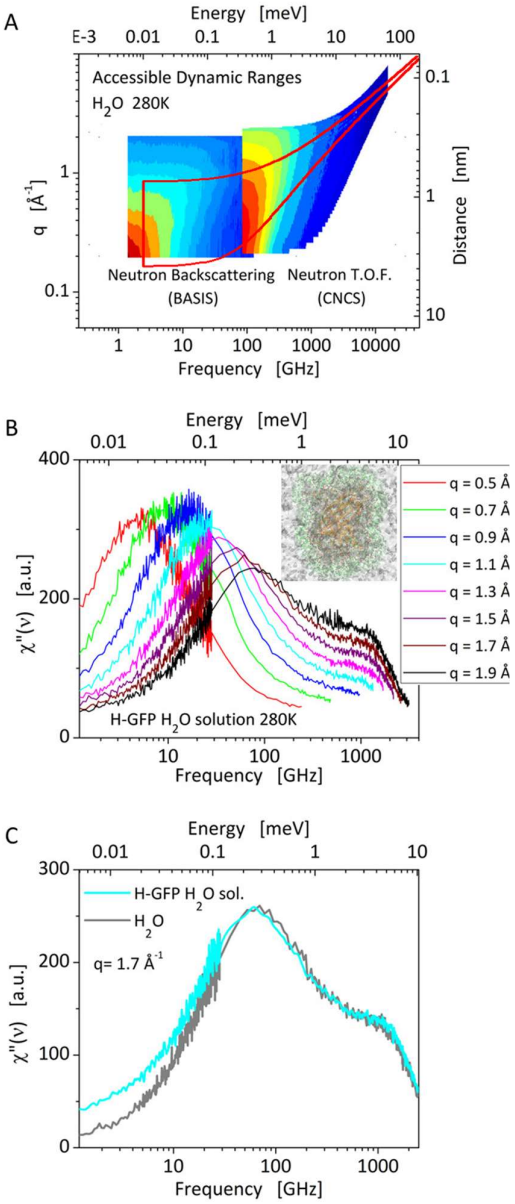

Fig. 7. Broadband neutron scattering capabilities are highly desirable to study the dynamics of water. (A) Recent work studying water hydrating Green Fluorescent Protein was compelled to utilize multiple spectrometers to achieve an experimental window covering the ns-ps dynamics of water. The capabilities of BWAVES would be an ideal fit for such studies. (B) Currently, Q-resolved spectra must be sliced and stitched in a cumbersome process from instruments with mismatched resolution and dynamic window. (C) Ultimately, this window is important to probe different water populations around model biomolecules. The data are adapted from [23].

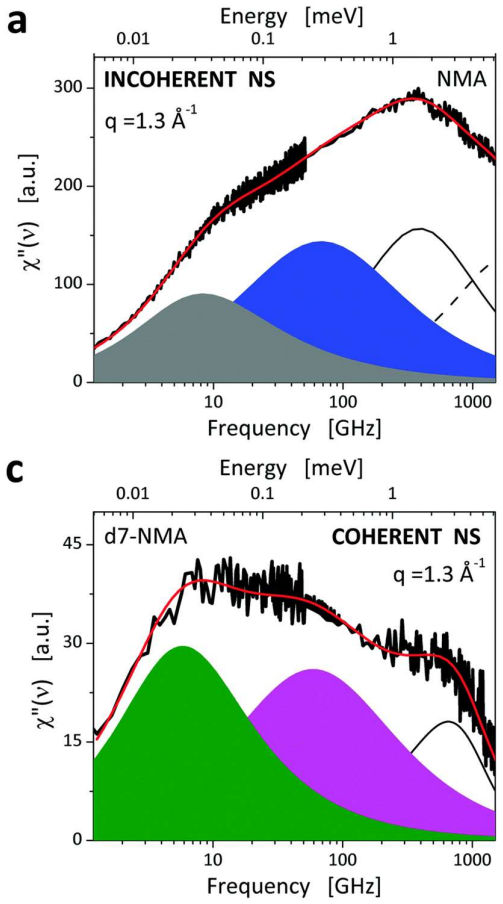

Fig. 8. Fitting of inelastic neutron scattering spectra from n-methylacetamide. Top: incoherent spectra, four components. Bottom: coherent spectra, three components. Reprinted with permission from [26]. Copyright 2017 The Royal Society of Chemistry.

the geometry of the lipid motion. It is likely that the lipid dynamics is best described as motion within a cylinder, yet the gap in the Q-range between the NSE and BASIS data leaves uncertainty regarding the effective cylinder dimensions. BWAVES, due to its capability of selecting long final wavelength (thus, lower Q and higher energy resolution) when operated in a "booster" mode, will be able to close the gap in the Q-range between NSE and BASIS and allow unequivocal determination of the geometry of the lipid motion.

While understanding cooperativity and heterogeneity in the dynamics of liquids and polymers remains a great scientific challenge, the dynamics of water, especially in confined space and at interfaces, is critical for a wide range of industrial and bio-medical applications and is a topic of equally active discussion [19-22]. For example, dielectric spectroscopy detects the main relaxation process in bulk water on the time scale ~10 ps, while light, neutrons and X-ray scattering detect the main structural relaxation on the time scale ~

1 ps [19-22]. BWAVES may resolve this conflict and is positioned to become an invaluable tool in hydration

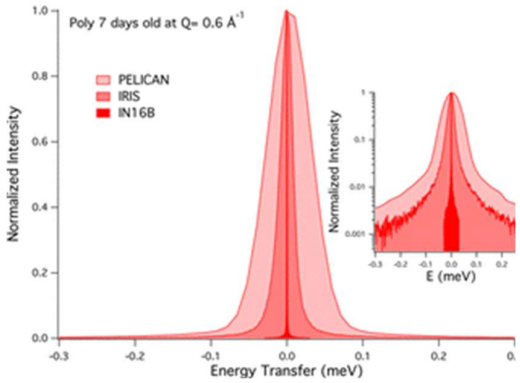

Fig. 9. Dynamics of aqueous polyacrylic acid in dental restorative cements: QENS spectra collected at backscattering and time-of-flight spectrometers. Reprinted with permission from [27]. Copyright 2018 American Chemical Society.

studies, increasing the quality and throughput of experimental studies of water dynamics, with the experimental window overlapping the coupled translational and rotational motions of water on the nanosecond to picosecond timescale as well as with vibrational modes.

The ability to capture the relevant water motions in a single experiment immediately reduces the difficulty of the experiment and ambiguity associated with combining information obtained on multiple spectrometers. For example, Fig. 7 presents the overlap of the current SNS QENS-capable spectrometers (BASIS and the cold neutron chopper spectrometer, CNCS) used for the study of water dynamics [23] in comparison to the proposed capabilities of BWAVES. It should be noted that explicit fits of QENS data collected at BASIS (±0.1 meV only) with more than 2 dynamic components have been infrequent, as such fits are difficult to carry out [24,25]. Another illustrative example of multi-component dynamic data (also collected at BASIS and CNCS), for which BWAVES would become a one-stop spectrometer, is given by a hydrogen-bonding liquid, n-methylacetamide (NMA) which is a model system for the peptide group (Fig. 8, [26]).

Studies of vibrational dynamics in soft matter, such as dental restorative cements [27], are presently championed at SNS by the VISION vibrational spectrometer. In such complex systems functionality is related to relaxational-translational molecular dynamics, and without a spectrometer with the exceptional characteristics of BWAVES, characterization of molecular dynamics again requires the use of many spectrometers. In the example presented in Fig. 9, four spectrometers were used at four different user facilities: in the USA, Australia, France, and the UK. Besides the logistical problems, in this case the traditional approach presents great challenges related to sample ageing, which is not uncommon in soft matter studies. When the experiments are designed to probe the molecular dynamics in the sample as a function of curing time (Fig. 9), the benefits of a single spectrometer capable of measuring relaxational-translational and vibrational dynamics simultaneously, such as BWAVES, are obvious.

2.2 Chemical spectroscopy

Understanding proton and ion dynamics in liquids,

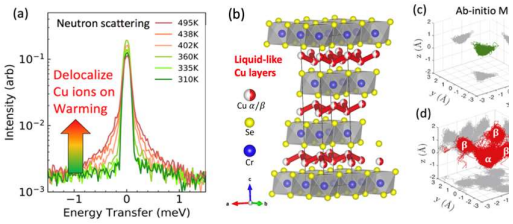

Fig. 10. (a) Quasi-elastic neutron scattering signal showing delocalization of Cu ions with increasing temperature (broadening of central peak). (b) Layered structure of $CuCrSe_2$, showing liquid-like Cu layers in superionic phase above 365 K. (c,d) Ab-initio MD calculations of Cu ion trajectory, showing delocalization across α and β sites at high T (adapted from [58]).

solids and polymers is another example of a scientific

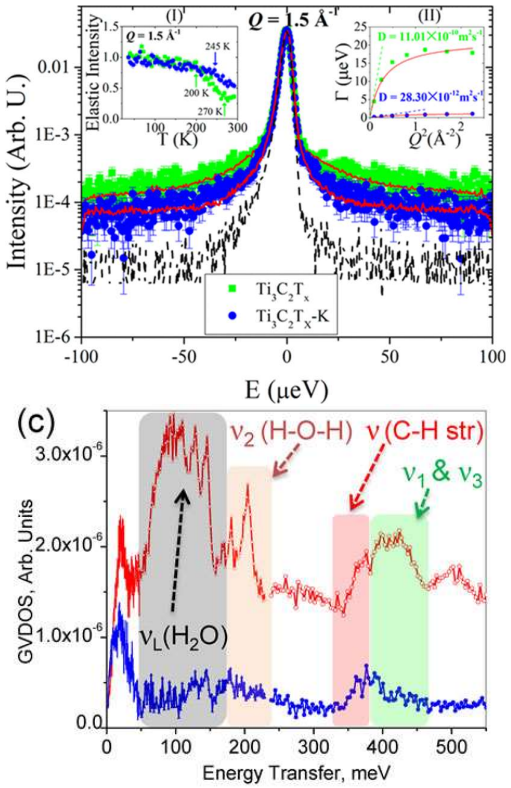

Fig. 11. Top: QENS spectra of MXenes samples measured at BASIS. Reprinted with permission from [77]. Copyright 2016 American Chemical Society. Bottom: the generalized vibrational density of states of MXene samples before (red curve) and after (blue curve) annealing, from the INS spectra measured at SEQUOIA. Reprinted with permission from [78]. Copyright 2014 American Chemical Society.

topic that can benefit tremendously from use of

broadband neutron scattering. For instance, superionic conductors (SICs) are unique solid materials in which a

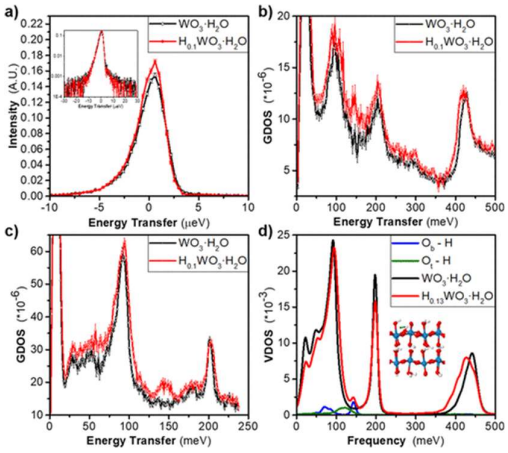

Fig. 12. Confined interlayer water in tungsten oxide hydrates enables fast highly reversible proton intercalation. (a) QENS (BASIS) of an electrode in the pristine, $WO_3 \cdot H_2O$, black, and intercalated, $H_{0.1}WO_3 \cdot H_2O$, red, states at T = 300 K. (b-c) INS (SEQUOIA) of the same electrodes at T = 5 K. (d) AIMD simulations of the vibrational density of states show the effect of protons at the terminal (O_t, green) and bridging (O_b, blue) oxygen atoms to the overall spectrum. Reprinted with permission from [79]. Copyright 2019 American Chemical Society.

portion of the structure becomes liquid-like at high temperatures (often above a phase transition), with

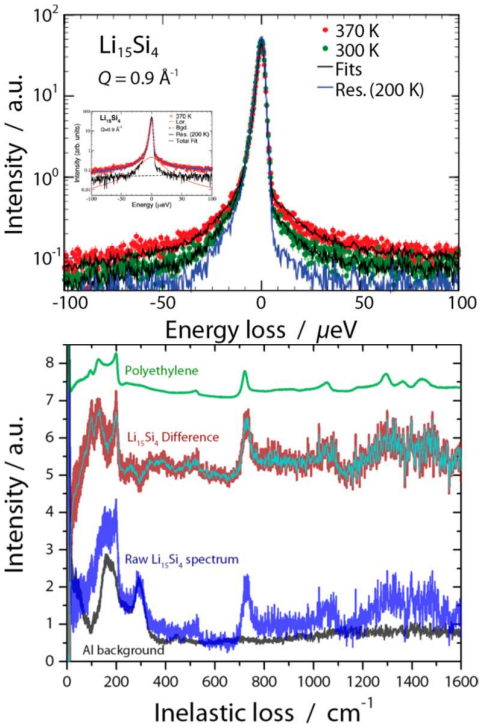

Fig. 13. QENS (top) and INS (bottom) spectra measured from an amorphous Li_xSi anode material. Reprinted with permission from [80]. Copyright 2017 American Chemical Society.

mobile ions acquiring diffusivities similar to liquid water at room temperature (D ~ 10^{-5} cm^2 s^{-1}). Steady interest in these systems [28-35] has spiked recently because of their promising applications as solid-state electrolytes for safer rechargeable batteries [36-46], as promising new thermoelectric materials [47-51], or as solid-oxide fuel-cells [52-54]. However, because of their intermediate nature between the solid and liquid states, SICs exhibit highly complex atomic dynamics involving many intricate processes ranging from solid-like phonons to liquid-like diffusion, which operate across multiple time and length scales [30,42,55,56]. Hence, the thermodynamic and transport properties of SICs remain poorly understood [56]. For example, two recent studies of atomic dynamics in the superionic "phonon-liquid electron-crystal" thermoelectric compounds $AgCrSe_2$ [57] and $CuCrSe_2$ [58] arrived at different conclusions regarding the atomistic processes dominating their thermal transport. These SICs are isostructural and both undergo phase transitions to a superionic state on heating, where Ag/Cu ions become highly mobile. Both exhibit ultra-low thermal conductivities (<1 W m^{-1} K^{-1} above 300 K) [49,59].

In Ref. [57] it was concluded that transverse acoustic phonons disappear in the superionic phase of $AgCrSe_2$, leading to a liquid-like thermal conductivity, while it was shown in [58] that long-wavelength acoustic phonons remain well-defined in the superionic phase of $CuCrSe_2$ but instead disorder and anharmonicity are strong sources of phonons scattering. BWAVES will be highly beneficial for resolving such controversies. The large dynamic range of BWAVES will enable simultaneous measurements of the signals that at present require two or three SNS spectrometers (e.g., BASIS, CNCS, ARCS, SEQUOIA, or VISION) to investigate both the QENS behavior (diffusion) and the lattice dynamics (phonons up to 10-100 meV) critical for understanding solid-state electrolytes for next-generation batteries. Moreover, the QENS signal from non-hydrogenous samples is relatively weak, and systematic studies (e.g., as a function of temperature and compositions) will be facilitated by the higher flux of BWAVES compared to BASIS.

As further example, recent breakthroughs in batteries [45] have achieved solid Li-ion or Na-ion SICs with ionic conductivities rivalling those of conventional organic liquid electrolytes [36,41,60-65]. These could replace liquid electrolytes to improve safety and boost energy density [40,65]. While many structural families of SICs have been uncovered (e.g. argyrodites [43,66], LISICON [67], NASICON [35], garnets [68], lithium nitrides [69,70], halides [71], and perovskites [72,73]), a clear understanding of how superionicity arises in structurally and chemically disparate compounds is still missing [39,45]. QENS is ideally matched to probe the dynamics of fast ions (~GHz), complementing measurements of THz lattice dynamics with INS, and BWAVES will be able to simultaneously measure both regimes in a single instrument setting, a unique feature not accessible with existing neutron spectrometers. Example QENS measurements across the superionic transition in $CuCrSe_2$ are shown in Fig. 10. The broadening of the QENS peak upon warming into the superionic phase (T > 365K) is the hallmark of increasing diffusion. The QENS data analysis will

directly estimate the ion diffusion and jump length from the Q dependence of the signal, and these results can be also combined with the analysis of phonons in the same measurements. Thus, BWAVES will open unprecedented opportunities for studying SICs.

The discovery of a novel class of 2D MXene materials [74-76] has revolutionized many applications and lead to an exponential growth in research on MXenes for electrochemical devices. The dynamics, both vibrational and diffusive, of water species in MXenes is critical for their electrochemical performance and long-term operational stability, and strongly depends on the water content and the intercalated ions. To date, MXenes have been studied separately at the SNS BASIS and SEQUOIA spectrometers (Fig. 11, [77,78]) using large-size aluminum sample holders for powders. The combination of QENS and INS capabilities with a small beam size in an open-tabletop sample geometry spectrometer such as BWAVES will facilitate simultaneous studies of vibrational and diffusive dynamics in real-life electrochemical devices, such as MXene-based supercapacitors, under operational condition (e.g., repeated charging-discharging).

There is a strong societal need for energy-related research and development, which requires comprehensive characterization of materials for batteries and supercapacitors. As an example, recent experiments at SNS (Fig. 12, [79]) measured intercalated proton dynamics in tungsten oxide hydrate electrodes. However, the characterization of the vibrational and stochastic energy landscape in these electrode materials relied on disparate measurements at BASIS at 300 K and SEQUOIA at 5 K, and possible soft dynamic modes could not be evaluated at all. The temperature-dependent QENS and INS measurements at BWAVES will provide thorough characterization of the vibrational and stochastic energy landscape in electrode materials, which feature multiple hydrogen-bearing species such as structural water molecules, hydration water molecules, and intercalated protons, each with its own dynamic characteristics. The power of temperature-dependent measurements for elucidating complex energy landscapes, which is specific to the inverted geometry spectrometers such as BWAVES, has been already mentioned above in the context of distinguishing between methyl groups with various rotational barriers (Fig. 4).

Similar to in situ studies of charging-discharging processes in real life supercapacitor devices, the small beam size and an open-tabletop geometry of BWAVES will enable in situ electrochemical studies of batteries under operation conditions. While it is common to use VISION for verification of the proton content in the materials with non-proton charge carriers studied separately at BASIS (e.g., Fig. 13 [80]), BWAVES will provide unprecedented opportunities for the simultaneous monitoring, in real time, of the mobility of Li charge carrier ions and the evolution of the vibrational dynamics in the matrix (e.g., battery anode) associated with the in-operando ion insertion.

2.3 Molecular dynamics in biological systems

Life, as we know it, is based on molecular motions.

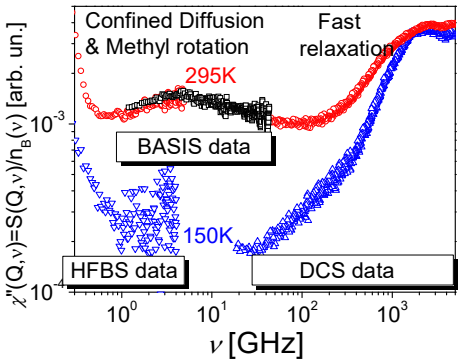

Fig. 14. Susceptibility spectra of protein lysozyme obtained by combination of data from 3 spectrometers, time-of-flight DCS (NIST), backscattering BASIS (SNS) and backscattering HFBS (NIST). Reprinted with permission from [86]. Copyright 2015 The Royal Society of Chemistry.

Biological materials are characterized by enormously complex energy landscapes, and the associated dynamic processes comprise a broad quasi-continuous spectrum of both vibrational and relaxation excitations. Due to the intricate coupling of biomolecules with their aqueous-based environment [81-86], the dynamics of which is already challenging to understand (Fig. 7), the dynamic landscape of hydrated / solvated biomolecules represents even higher level of complexity. Moreover, studies of living systems are challenged with the need to incorporate knowledge on multiple length and time scales. On length scales this involves a continuum from communities, to organisms to organs and down to cells and molecules. On time scales dynamic phenomena in a single protein occur on at least 17 decades of time (fs-10^2s). BWAVES acts in the multiscale research space, connecting phenomena over 4 decades of time, and promises thus to furnish vital information on connected and interdependent multiscale dynamical phenomena and forces at the molecular level of biology.

Neutrons have many desirable and unique properties as a probe of biomolecular dynamics, but the bandwidth limitations of classical neutron spectroscopy are problematic when the broad excitations of diffusive and relaxation motions need to be simultaneously probed. This is true in hard matter systems but is especially detrimental in studies of soft matter and biological systems, where the excitations are broad in energy space and oftentimes overlap with one another. This can, similarly to the above non-biological cases, lead to misinterpretations and ambiguity in analysis of neutron scattering data. As a typical example, analysis of the broad relaxation spectra in a protein required measurements on 3 different spectrometers (Fig. 14, [86]) - a very time and sample consuming process. BWAVES, due to its broad dynamic range, will address this problem. Many experimental techniques can measure longer time dynamics (μs and longer) than BWAVES. However, it remains a great challenge to understand the details of dynamic processes on

microscopic time scales (~fs-ns), which are collective, cooperative, and intrinsically heterogeneous. These timescales directly probe the interactions intrinsic in the molecular structure of biomolecules and their assemblies.

Moreover, the internal motions of protein on the timescales accessible to BWAVES are critical to the *in silico* drug discovery procedure of ensemble docking [87,88], in which the dynamic nature of drug binding sites is taken into account in virtual high-throughput screening. To this end, perhaps nothing can illustrate better the importance of neutron spectroscopy for probing the dynamics in complex biosystems than the pandemic caused by COVID-19 virus. The SARS-CoV-2 coronavirus, the causative agent of COVID-19, contains a spike protein, which is a molecular machine for binding to and penetrating human host cells (Fig. 15, [89,90]). Small-molecule drugs binding within the S-protein-human ACE2 interface may prevent this infectious step, and understanding the flexibility of the drug binding sites is essential to the design process. Other SARS-CoV-2 proteins can also be examined, and, to help derive pan-coronavirus treatments for the coming decades, binding site flexibilities of the entire suite of non-structural viral proteins should be derived. INS and QENS measurements at BWAVES will be essential for studies investigating protein-ligand binding.

Further, the mechanics of infection and viral particle assembly requires conformational changes in the protein machines responsible for them. Understanding these steps in the viral lifecycle will require characterization of the anharmonic dynamics responsible for the mechanical soft modes involved. Inelastic neutron scattering spectra ranging from the femtosecond to nanosecond timescale will be invaluable in this regard as they will provide information on the elastic properties of this molecular machine in various states and their perturbations due to the interactions with potential drugs. Moreover, on a fundamental level, the time- and geometry-dependence of motions detectable by BWAVES will be of great help in deciphering the relationship between non-ergodic, ageing, internal protein dynamics [91] in single proteins as determined by molecular dynamics simulation and single-molecule FRET and ensemble characteristics measured by BWAVES. An open question in the studies of biological systems, from single proteins to complex systems as bacteria or cells, concerns the relaxation processes self-similarities over many decades in time, for which there are hints reported in the literature [92]. To obtain information over such broad time ranges, one needs to use spectrometers giving access to complementary time domains, or even better an instrument such as BWAVES, which permits us to see a broad energy-time domain at once, avoiding problems due to different normalizations.

Another biologically important field is the dynamics of hydration water of macromolecules, microbial envelopes, plant cell wall polymers, and many other systems. The structurally and dynamically perturbed hydration shells of proteins and other biomolecules have a strong influence on their function and stability. Many recent studies have focused in great

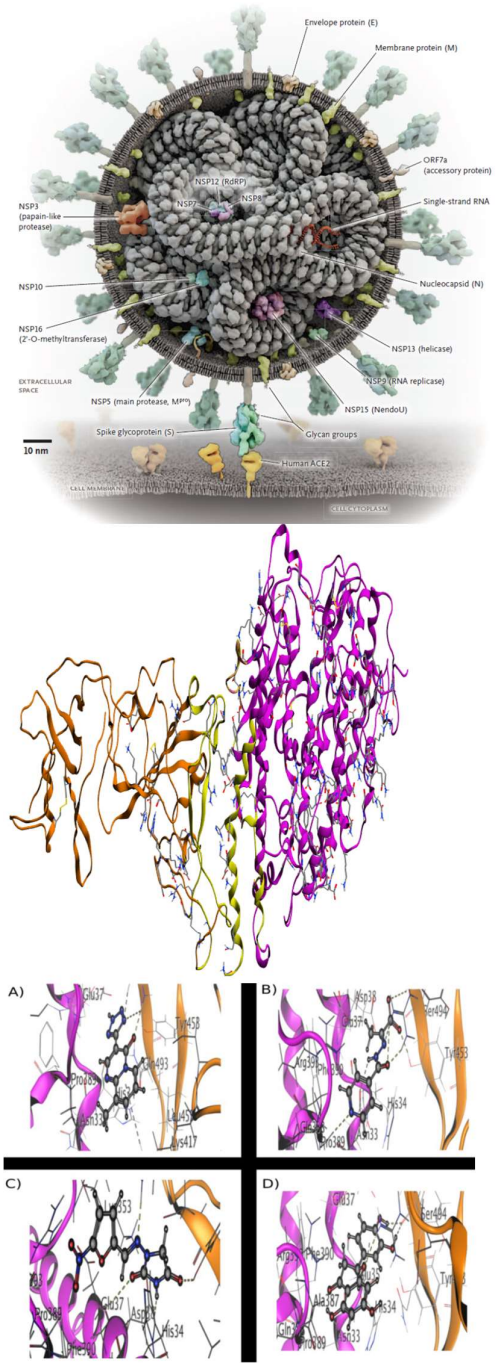

Fig. 15. Top: SARS-CoV-2 virus (reprinted with permission from [89]. Copyright 2020 American Chemical Society). Middle: the S-protein of SARS-CoV-2 and human ACE2 receptor complex. Orange ribbons: the S-protein, purple: the ACE2, yellow: the interface targeted for docking (reproduced from [90]). Bottom: Four of the top scoring small-molecules binding within the S-protein-ACE2 interface. A) pemirolast. B) isoniazid pyruvate. C) Nitrofurantoin. D) Eriodictyol. Orange ribbons: the S-protein, purple: the ACE2 receptor (reproduced from [90]). These calculations required a knowledge of the dynamics of the target proteins on the BWAVES time scales.

depth on providing a description of hydration water

dynamics using neutron scattering methods [93-95]. Neutron scattering approaches can quantify the number of molecules perturbed by the presence of a biomolecule and the degree of the perturbation. The recent investigation of water dynamics in crowded solutions of green fluorescent protein (Fig. 7) is a good example [23], where the spectral analysis revealed that slightly less than two shells (~5.5 Å) of water were perturbed by the presence of the protein, with dynamics a factor of 2−10 times slower than bulk water. These results help clarify the seemingly conflicting range of values reported for hydration water retardation as a logical consequence of the different length scales probed by the

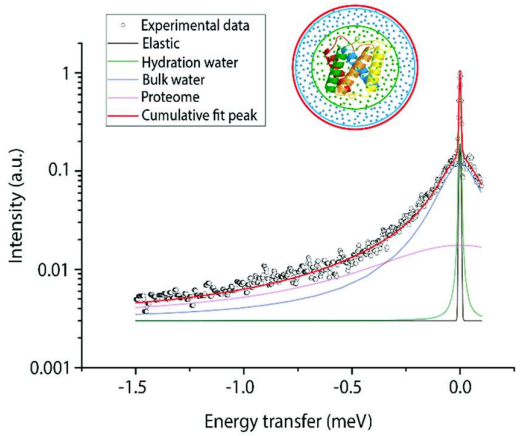

Fig. 16. Normalized QENS spectra and fit for *T. barophilus* at 298 K, 40 MPa and Q = 0.96 Å^{-1} on a semi-logarithmic scale. Scheme in the red circle represents the different populations studied, the ribbons represent a protein, and the dots represent water molecules (green for hydration water and blue for bulk water). Reprinted with permission from [105]. Copyright 2019 The Royal Society of Chemistry.

analytical techniques used. Neutrons not only provide a detailed description of water dynamics but do so in a way which adds clarity to the broad community studying the question with other approaches. Even more challenging are studies of water dynamics in cells, where the experimentally determined parameters reveal that hydration water dynamics strongly depend on the confinement environment (size, pH, hydrophilic or hydrophobic surface, etc.) [96]. No single experimental technique can give a full picture of such intricate dynamics, but the broadband capability of BWAVES will provide the most comprehensive information yet.

The study of anticancer drug effects at the cellular level is another fascinating example where the need to measure both vibrational and relaxational phenomena in a single spectrum is critical [97]. BWAVES will make this type of measurement possible. By scrutinizing the effect of distinct chemotherapeutic agents on the water dynamics of different cell lines, the active water role in living organisms over many scales of time and distance will be finally re-evaluated [98]. BWAVES capabilities will offer unparalleled advantages for cellular water investigations under various environmental conditions using neutron scattering (not attainable by NMR [99]) and consolidate the role of neutron scattering in cell-based drug characterization. BWAVES will also play a pivotal role in biotechnology and biomedicine by allowing – with the aid of specialized sample environment [100] – studies of changes in the cellular water dynamics caused by stimuli-responsive drug delivery systems that respond to heat, pH, light, magnetic and/or electrical field. These smart bionanomaterials, where controlled and long-term drug release is enabled by the action of an external stimulus, offer the promise of treatments for chronic diseases. Activating these materials using electrical signals would make this technology easy to generate and control [101,102].

Even though the movement of ions and water dipoles is postulated to be important in the chemical pathway of electroporation (a microbiology technique that uses electrical field to increase the permeability of the cell membrane) and electroosmotic flow (movement of a liquid in a porous material or biological membrane under the influence of an electric field), research gaps still need to be closed to advance this technology. For instance, how are the transport mechanisms of water or ions affected by an applied electric field? Answering this question is key for developing novel hybrid organic-inorganic electric field responsive drug delivery systems. Here, again, the need to measure both vibrational and relaxational phenomena in a single spectrum is crucial [103,104]. The unique ability of

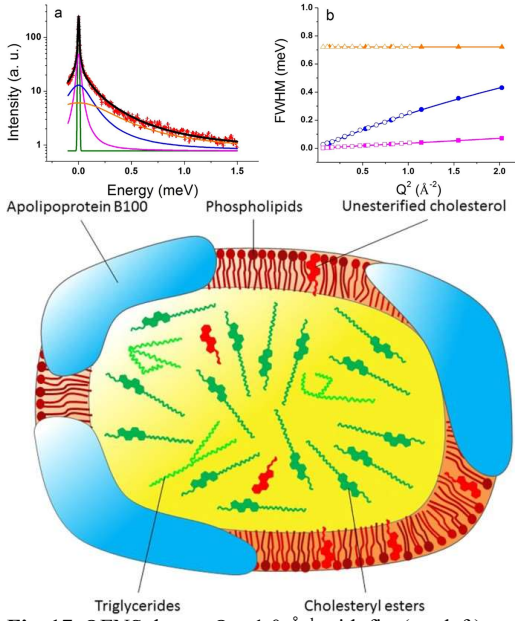

Fig. 17. QENS data at Q = 1.0 Å^{-1} with fits (top left) and the associated signal broadening (top right) from lipoprotein particles (bottom) measured at 310 K and 20 bar (reprinted with permission from [106]). The FWHM values of the three Lorentzian distributions as a function of Q-squared as presented in the top right panel were obtained at IN5, ILL (smaller Q-range, open symbols) and IN6, ILL (filled symbols) and fitted using a translational diffusion model (magenta points), a jump-diffusion model (blue points), and a rotational diffusive model (orange points).

neutron scattering to study encapsulated drugs at the molecular level will lead to deeper understanding of their mobility/release dynamics. Being able to predict

release profiles of complexed drugs is one of the greatest challenges faced by pharmaceutical technology. Such an understanding would bring to light the possibility of tailoring the drug release rate in accordance with the desired effect, and a combination of density functional theory calculations with incoherent inelastic spectroscopy and state of the art sample environment is a promising approach to overcome this challenge using BWAVES, facilitated by the open sample geometry aiding stimuli application.

The ability of BWAVES to fully characterize the dynamics of a sample in one shot is of critical importance for studies involving stimulus-induced response, because it ensures that the dynamics at all energy transfers is always probed in the identical state of the sample immediately before, during, and after the stimulus application. When carried out at different spectrometers, processes such as in situ hydration/dehydration and drug delivery would require full reproducibility of the external stimulus application that is hard to achieve in practice, thus requiring stitching together data sets collected not necessarily under the identical conditions. This exacerbates the already mentioned issues of the mismatched Q ranges and arbitrary data normalization from different spectrometers. Simultaneous measurements over the full dynamic range, as allowed by BWAVES, will resolve this problem of reproducible stimuli application, which grows more challenging with the increasing complexity of the systems under investigation.

Understanding biological complexity and metabolism in plants and microbes is a further grand challenge. Connecting the molecular scale dynamics of hydrogen atoms or collective fluctuations of biological structures to organism level phenomena requires advances in the tools for assessing molecular motions, such as provided by BWAVES. Rapidly capturing broad spectral snapshots of molecular motions is crucial for understanding differences in molecular motions based on different biological stimuli. Furthermore, studies of complex systems are favored by open tabletop BWAVES design capable of accommodating complex sample environments. A more open sample environment allows for sample interaction with light, added chemicals (salts, metabolites, etc.), and pressure, to name a few. Because biological systems are constantly changing, it is crucial to monitor samples in the course of experiments. Parameters such as optical density, fluorescence, or settling of cells out of solution must be monitored to ensure that changes in dynamics are representative of real phenomena. Thus, easy access to the sample (including access by optical probes) will be a highly beneficial feature of BWAVES design.

Investigation of very complex systems such as prokaryotes can provide information on adaptation mechanisms to extreme external conditions such as high temperature, pressure, and salinity. In recent studies, QENS data were collected on *Thermococcus barophilus*, a microbe living in the deep sea close to hot vents. Fig. 16 [105] shows that, besides the elastic contribution, there are several dynamic components in the cellular dynamics, corresponding to bulk and hydration water and the proteome. These contributions were visible within the rather limited energy transfer range of the spectrometer IN5 (ILL), but the correct interpretation of the two components arising from water required other measurements on IN6 (ILL). Therefore, for these relaxational studies, a broadband range spectrometer is again imperative. In addition, it is desirable to probe low-energy vibrational dynamics simultaneously and on the same samples, as they are very difficult and expensive to produce. Hence a spectrometer that resolves all the relaxational components shown in this spectrum, but also goes much beyond the energy transfer shown here, becomes mandatory. Moreover, modern MD simulations allow a combination of all-atom and coarse-grain approaches, permitting to reasonably model bacteria as *Eschericia coli* and therefore to compare the results from vibrational and local motions to global movements, thus allowing to make progress on both the experimental and simulations sides. Therefore, an instrument as BWAVES will make a dramatic difference in this kind of studies of microorganisms.

Another example where dynamics influences function is human plasma lipoproteins - macromolecular assemblies of lipids and proteins which transport lipids through blood circulation. The main function of low-density lipoproteins (LDLs) is the transportation of

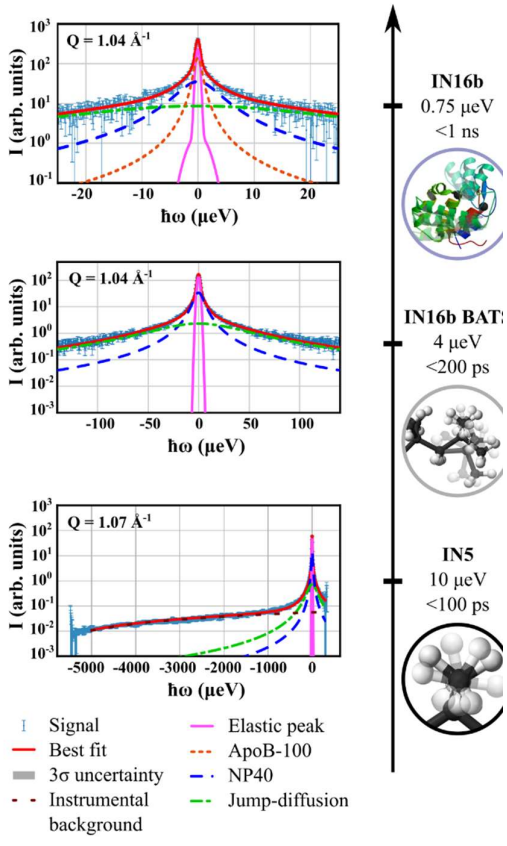

Fig. 18. An example of apo B-100/NP40 data fitting (modified from [107]) on 3 spectrometers (IN16b - top; IN16b BATS - middle; IN5 - bottom) at Q = 1.05 Å^{-1}.

cholesterol from the liver to peripheral tissue. LDL particles (Fig. 17, [106]) comprise a combination of lipids and a single copy of a protein, apolipoprotein

B100 (apoB100). They have a hydrophobic core and an amphiphilic shell. While the core hosts cholesteryl esters, triglycerides, and parts of the unesterified cholesterol, the shell consists of a phospholipid monolayer, unesterified cholesterol, and the amphipathic apoB100 molecule wrapped around the surface. LDL is a key contributor to lipid deposition in the arteries leading to atherosclerosis. Exploration of the dynamical features of the LDL particles with either a normal or triglyceride-rich lipid composition is essential for accurate modeling and understanding of the LDL interactions with various biological environments in vivo. The complexity of the lipid dynamics in the LDL particles has necessitated the use of different neutron spectrometers for the global fit of the QENS spectra [106]. However, because all the dynamic components have been demonstrated to contribute prominently to the QENS spectra measured at Q = 1.0 $Å^{-1}$ and below (Fig. 17), BWAVES will enable single-spectrometer measurements of lipoprotein dynamics, while its open-tabletop geometry will facilitate the in situ control over the physiologically relevant conditions of the lipoprotein's host solutions.

One moiety of LDL, the apolipoprotein B-100 (apo B-100), has been scarcely studied. Due to its amphiphilic nature, it is partly located at the surface of the LDL and partly embedded in its phospholipid monolayer. Therefore, it has characteristics close to classical membrane proteins and is very difficult to extract from LDL, and thus its solubilization is associated with detergent remaining in the sample. Recently, the dynamics of apo B-100 and its detergent, Nonidet P-40 (NP40) were separated using incoherent neutron scattering experiments [107] but through a combination of measurements on three different spectrometers at ILL: IN5, IN16b in BATS mode, and IN16b (see Fig. 18). This approach allowed the motions of the detergent alone to be identified, and, by fixing some of the parameters, to separate the parameters specific to apo B-100. Such methodology can render studies of other membrane proteins achievable. The potential to collect all necessary data on one instrument, such as BWAVES, under the same conditions, would greatly simplify such measurements and improve data reliability.

3 Conclusion

BWAVES will be capable of simultaneous characterization of vibrational and relaxational spectra in an enormous range of soft matter systems. Herein we discussed the benefits of this approach using numerous examples from recent neutron spectroscopy studies in a broad range of systems. We reiterate the main characteristics of BWAVES, which we have discussed in the paper, as follows:

(1) Measurements of continuous spectra covering energy transfers from below 0.010 meV to above 500 meV.

(2) The only currently proposed inverted geometry spectrometer for SNS STS, well suited to map relaxational excitations gradually emerging as a function of temperature.

(3) A small beam size (5 mm by 5 mm).

(4) An open-tabletop sample geometry instrument.

(5) The flexibility to function as the workhorse spectrometer at SNS STS for studies of chemical, soft matter, and biological systems.

The importance of the first three features of BWAVES can be demonstrated using recent studies [14,108,109] of several potential therapeutic agents for COVID-19 treatment, which were carried out at SNS in the Spring of 2020. These studies required the use of BASIS, CNCS, VISION, and SEQUOIA spectrometers for different measurements spanning several weeks. These measurements could have been completed much more readily and efficiently with the use of a single broadband spectrometer such as BWAVES. A broadband inverted geometry spectrometer such as BWAVES would be capable of thorough mapping of the rotational potentials of side groups in molecular compounds such as anti-COVID-19 drugs and other antiviral agents, which proved elusive to achieve with the existing spectrometers (Fig. 4, [14]). Further, it was necessary to bypass several promising drug candidates altogether because they were available only in microgram quantities, which could not be measured using the existing spectrometers with an incident beam size of ca. 10 cm^2 or larger. BWAVES will enable these types of samples to be probed, with its smaller beam size and a high neutron flux.

While the implications of the first three features of BWAVES are well understood and appreciated, the latter points represent novel features of BWAVES that remain to be explored by the community. Never before has a broadband high energy-resolution spectrometer been built with an open sample geometry more resembling that of neutron reflectometers than traditional neutron spectrometers.

An important element of BWAVES operation will be integration with a range of computational and experimental techniques in multimodal studies of important soft matter systems. For example, the convenient and routine application of external stimuli to samples, including optical probes, will greatly broaden the usefulness of the neutron measurements and will and enable the users, both experienced and new, to expand the application of neutron scattering in ways not possible with today's neutron spectrometers. Such expansions may be difficult to appreciate at present. Furthermore, the dynamic range of BWAVES mirrors that accessible to molecular dynamics simulation and developments in the latter utilizing high-performance computing need rigorous experimental testing. BWAVES, by virtue of its direct probing of dynamics on a wide range of timescales, will provide the necessary constraints.

All in all, it may be fair to describe BWAVES as a workhorse spectrometer at SNS STS that will provide a gamut of unprecedented characterization capabilities to a broad user community. Serious consideration needs to be given to the future computational approaches suitable to model both QENS and INS measured signals, not separately, but within the same spectra.

The design of BWAVES has been the result of efforts by many contributors. This research used resources of the Spallation Neutron Source Second Target Station Project at Oak Ridge National Laboratory (ORNL). ORNL is managed by UT-Battelle LLC for DOE's Office of Science, the single largest supporter of basic research in the physical sciences in the United States. The operation and user program at the Spallation Neutron Source is supported by the Scientific User Facilities Division, Office of Basic Energy Sciences, U.S. Department of Energy. OD acknowledges support from the US Department of Energy, Office of Science, Basic Energy Sciences, Materials Sciences and Engineering Division, under Award No. DE-SC0019978. GJS gratefully acknowledges funding by the U.S. Department of Energy under grant DE-SC0019050. The United States Government retains and the publisher, by accepting the article for publication, acknowledges that the United States Government retains a non-exclusive, paid-up, irrevocable, world-wide license to publish or reproduce the published form of this manuscript, or allow others to do so, for the United States Government purposes.

References

1. E. Mamontov, K.W. Herwig, Rev. Sci. Inst. **82**, 085109 (2011)
2. K. Shibata, N. Takahashi, Y. Kawakita, M. Matsuura, T. Yamada, T. Tominaga, W. Kambara, M. Kobayashi, Y. Inamura, T. Nakatani, K. Nakajima, M. Arai, JPS Conf. Proc. **8**, 036022 (2015)
3. B. Frick, E. Mamontov, L. van Eijck, T. Seydel, Z. Phys. Chem. **224**, 33-60 (2010)
4. M. Appel, B. Frick, A. Magerl, Physica B: Condens. Matter **562**, 6-8 (2019)
5. D. Colognesi, M. Celli, F. Cilloco, R. J. Newport, S.F. Parker, V. Rossi-Albertini, F. Sacchetti, J. Tomkinson, M. Zoppi, Appl. Phys. A: Mater. Sci. Process. **74**, S64-S66 (2002)
6. P.A. Seeger, L.L. Daemen, J.Z. Larese, Nucl. Instrum. Methods Phys. Res. A **604**, 719-728 (2009)
7. E. Mamontov, Nucl. Instrum. Methods Phys. Res. A **759**, 83-91 (2014)
8. E. Mamontov, C. Boone, M.J. Frost, K.W. Herwig, T. Huegle, J. Lin, B. McCormick, W. McHargue, A. D. Stoica, P. Torres, W. Turner, Rev. Sci. Inst. **93**, 045101 (2022)
9. P.K. Willendrup, K. Lefmann, J. Neutron Res. **22**, 1-16 (2020)
10. P.K. Willendrup, K. Lefmann, J. Neutron Res. **23**, 7-27 (2021)
11. J.Y.Y Lin, H.L. Smith, G.E. Granroth, D.L. Abernathy, M.D. Lumsden, B. Winn, A.A. Aczel, M. Aivazis, B. Fultz, Nucl. Instrum. Methods Phys. Res. A **810**, 86-99 (2016)
12. J.Y.Y Lin, F. Islam, G. Sala, I. Lumsden, H. Smith, M. Doucet, M.B. Stone, D.L. Abernathy, G. Ehlers, J.F. Ankner, G.E. Granroth, J. Phys. Communications **3**, 085005 (2019)
13. D.W. Kneller, O. Gerlits, L.L. Daemen, A. Pavlova, J.C. Gumbart, Y.Cheng, A. Kovalevsky, Phys. Chem. Chem. Phys. **24**, 3586-3597 (2022)
14. E. Mamontov, Y.Cheng, L.L. Daemen, A.I. Kolesnikov, A.J. Ramirez-Cuesta, M.R. Ryder, M.B. Stone, Chem. Phys. Lett. **777**, 138727 (2021)
15. A.P. Holt, V. Bocharova, S. Cheng, A.M. Kisliuk, G. Ehlers, E. Mamontov, V.N. Novikov, A.P. Sokolov, Phys. Rev. Mater. **1**, 062601 (2017)
16. K.J. Bichler, B. Jacobi, V. Garcia Sakai, A. Klapproth, R.A. Mole, G.J. Schneider, Macromolecules **53**, 9553-9562 (2020)
17. K.J. Bichler, B. Jacobi, V. Garcia Sakai, A. Klapproth, R.A. Mole, G.J. Schneider, Nano Lett. **21**, 4494-4499 (2021)
18. S. Gupta, G.J. Schneider, Soft Matter **16**, 3245-3256 (2020)
19. J.S. Hansen, A. Kisliuk, A.P. Sokolov, C. Gainaru, Phys. Rev. Lett. **116**, 237601 (2016)
20. A. Arbe, P. Malo de Molina, F. Alvarez, B. Frick, J. Colmenero, Phys. Rev. Lett. **117**, 185501 (2016)
21. T. Iwashita, B. Wu, W.R. Chen, S. Tsutsui, A.Q.R. Baron, T. Egami, Sci. Advances **3**, e1603079 (2017)
22. T. Egami, Y. Shinohara, Mol. Phys. **117**, 3227-3231 (2019)
23. S. Perticaroli, G. Ehlers, C.B. Stanley, E. Mamontov, H. O'Neill, Q. Zhang, X.L. Cheng, D.A. Myles, J. Katsaras, J.D. Nickels, J. Am. Chem. Soc. **139**, 1098-1105 (2017)
24. D.V. Wagle, G.A. Baker, E. Mamontov, J. Phys. Chem. Lett. **6**, 2924-2928 (2015)
25. C.Z. Xie, S.M. Chang, E. Mamontov, L.R. Stingaciu, Y.F. Chen, Phys. Rev. E **101**, 012416 (2020)
26. S. Perticaroli, B. Mostofian, G. Ehlers, J.C. Neuefeind, S.O. Diallo, C.B. Stanley, L. Daemen, T. Egami, J. Katsaras, X. Cheng, J.D. Nickels, Phys. Chem. Chem. Phys. **19**, 25859-25869 (2017)
27. M.C. Berg, A.R. Benetti, M.T.F. Telling, T. Seydel, D. Yu, L.L. Daemen, H.N. Bordallo, ACS Appl. Mater. Sci. **10**, 9904-9915 (2018)
28. G.D. Mahan, W.L. Roth, Superionic conductors: [proceedings]. Physics of solids and liquids. 1976, New York: Plenum Press. xvi, 438 p.
29. M.B. Salamon, Physics of superionic conductors. Topics in current physics. 1979, Berlin ; New York: Springer-Verlag. xii, 255 p.
30. J.B. Boyce, B.A. Huberman, Phys. Rep. - Review Section of Physics Letters **51**, 189-265 (1979)
31. W. Dieterich, J. Stat. Phys. **39**, 583-596 (1985)
32. K. Wakamura, K. Hirokawa, H. Shima, K. Takarabe, Solid State Ion. **40-1**, 331-333 (1990)
33. K. Wakamura, F. Miura, A. Kojima, T. Kanashiro, Phys. Rev. B **41**, 2758-2762 (1990)

34. K. Wakamura, K. Hirokawa, K. Orita, J. Phys. Chem. Solids **57**, 75-80 (1996)
35. A. Martinez-Juarez, C. Pecharroman, J.E. Iglesias, J.M. Rojo, J. Phys. Chem. B **102**, 372-375 (1998)
36. N. Kamaya, K. Homma, Y. Yamakawa, M. Hirayama, R. Kanno, M. Yonemura, T. Kamiyama, Y. Kato, S. Hama, K. Kawamoto, A. Mitsui, Nat. Mater. **10**, 682-686 (2011)
37. S.P. Ong, Y.F. Mo, W.D. Richards, L. Miara, H.S. Lee, G. Ceder, Energy Environ. Sci. **6**, 148-156 (2013)
38. Y. Wang, W.D. Richards, S.P. Ong, L.J. Miara, J.C. Kim, Y.F. Mo, G. Ceder, Nat. Mater. **14**,1026 (2015)
39. J.C. Bachman, S. Muy, A. Grimaud, H.H. Chang, N. Pour, S.F. Lux, O. Paschos, F. Maglia, S. Lupart, P. Lamp, L. Giordano, Y. Shao-Horn, Chem. Rev. **116**, 140-162 (2016)
40. J. Janek, W.G. Zeier, Nat. Energy **1**, 16141 (2016)
41. Y. Kato, S. Hori, T. Saito, K. Suzuki, M. Hirayama, A. Mitsui, M. Yonemura, H. Iba, R. Kanno, Nat. Energy **1**, 16030 (2016)
42. X.F. He, Y.Z. Zhu, Y.F. Mo, Nat. Commun. **8**, 15893 (2017).
43. M.A. Kraft, S.P. Culver, M. Calderon, F. Bocher, T. Krauskopf, A. Senyshyn, C. Dietrich, A. Zevalkink, J. Janek, W.G. Zeier, J. Am. Chem. Soc. **139**, 10909-10918 (2017)
44. T. Krauskopf, C. Pompe, M.A. Kraft, W.G. Zeier, Chem. Mater. **29**, 8859-8869 (2017)
45. A. Manthiram, X.W. Yu, S.F. Wang, Nat. Rev. Mater. **2**, 16103 (2017)
46. M.K. Gupta, J. Ding, N.C. Osti, D.L. Abernathy, W. Arnold, H. Wang, Z. Hood, O. Delaire, Energy Environ. Sci. **14**, 6554-6563 (2021)
47. H. Liu, X. Shi, F. Xu, L. Zhang, W. Zhang, L. Chen, Q. Li, C. Uher, T. Day, G.J. Snyder, Nat. Mater. **11**, 422-425 (2012)
48. K.S. Weldert, W.G. Zeier, T.W. Day, M. Panthofer, G.J. Snyder, W. Tremel, J. Am. Chem. Soc. **136**, 12035-12040 (2014)
49. F. Damay, S. Petit, S. Rols, M. Braendlein, R. Daou, E. Elkaim, F. Fauth, F. Gascoin, C. Martin, A. Maignan, Sci. Rep. **6**, 23415 (2016)
50. T.P. Bailey, C. Uher, Current Opinion in Green and Sustainable Chemistry **4**, 58-63 (2017)
51. A.J.E. Rettie, J. Ding, X. Zhou, M.J. Johnson, C.D. Malliakas, N.C. Osti, D. Young Chung, R. Osborn, O. Delaire, S. Rosenkranz, M.G. Kanatzidis, Nat. Mater. **20**, 1683-1688 (2021)
52. A. Villesuzanne, W. Paulus, A. Cousson, S. Hosoya, L. Le Dreau, O. Hernandez, C. Prestipino, M.I. Houchati, J. Schefer, J. Solid State Electrochem. **15**, 357-366 (2011)
53. A. Perrichon, A. Piovano, M. Boehm, M. Zbiri, M. Johnson, H. Schober, M. Ceretti, W. Paulus, J. Phys. Chem. C **119**, 1557-1564 (2015)
54. X.Y. Li, N.A. Benedek, Chem. Mater. **27**, 2647-2652 (2015).
55. R. Hempelmann, Quasielastic neutron scattering and solid state diffusion. Oxford series on neutron scattering in condensed matter. 2000, Oxford: Clarendon Press. xii, 304 p.
56. Y.G. Zhou, S.Y. Xiong, X.L. Zhang, S. Volz, M. Hu, Nat. Commun. **9**, 4712 (2018)
57. B. Li, H. Wang, Y. Kawakita, Q. Zhang, M. Feygenson, H.L. Yu, D. Wu, K. Ohara, T. Kikuchi, K. Shibata, T. Yamada, X.K. Ning, Y. Chen, J.Q. He, D. Vaknin, R.Q. Wu, K. Nakajima, M.G. Kanatzidis, Nat. Mater. **17**, 226 (2018)
58. J.L. Niedziela, D. Bansal, A.F. May, J. Ding, T. Lanigan-Atkins, G. Ehlers, D.L. Abernathy, A. Said, O. Delaire, Nat. Phys. **15**, 73–78 (2019)
59. J. Ding, J.L. Niedziela, D. Bansal, J. Wang, X. He, A.F. May, G. Ehlers, D.L. Abernathy, A. Said, A. Alatas, Y. Ren, G. Arya, O. Delaire, Proc. Natl. Acad. Sci. U. S. A. **117**, 3930-3937 (2020)
60. P. Bron, S. Johansson, K. Zick, J. S. auf der Gunne, S. Dehnen, B. Roling, J. Am. Chem. Soc. **135**, 15694-15697 (2013)
61. A. Kuhn, V. Duppel, B.V. Lotsch, Energy Environ. Sci. **6**, 3548-3552 (2013)
62. A Kuhn, O. Gerbig, C.B. Zhu, F. Falkenberg, J. Maier, B.V. Lotsch, Phys. Chem. Chem. Phys. **16**, 14669-14674 (2014)
63. K. Xu, Chem. Rev. **104**, 4303-4417 (2004)
64. K. Xu, Chem. Rev. **114**, 11503-11618 (2014)
65. M. Armand, J.M. Tarascon, Nature **451**, 652-657 (2008)
66. H.J. Deiseroth, S.T. Kong, H. Eckert, J. Vannahme, C. Reiner, T. Zaiss, M. Schlosser, Angew. Chem.-International Edition **47**, 755-758 (2008)
67. A.R. Rodger, J. Kuwano, A.R. West, Solid State Ion. **15**, 185-198 (1985)
68. V. Thangadurai, S. Narayanan, D. Pinzaru, Chem. Soc. Rev. **43**, 4714-4727 (2014)
69. H. Yamane, S. Kikkawa, M. Koizumi, Solid State Ion. **25**,183-191 (1987)
70. W. Schnick, J. Luecke, Solid State Ion. **38**, 271-273 (1990)
71. W. Schmidt, H.D. Lutz, Berichte Der Bunsen-Gesellschaft – Phys. Chem. Chem. Phys. **88**, 720-723 (1984)
72. O. Bohnke, C. Bohnke, J.L. Fourquet, Solid State Ion. **91**, 21-31 (1996)
73. S. Stramare, V. Thangadurai, W. Weppner, Chem. Mater. **15**, 3974-3990 (2003)
74. M. Naguib, M. Kurtoglu, V. Presser, J. Lu, J. Niu, M. Heon, L. Hultman, Y. Gogotsi, M.W. Barsoum, Adv. Mater. **23**, 4248-4253 (2011)
75. M. Naguib, O. Mashtalir, J. Carle, V. Presser, J. Lu, L. Hultman, Y. Gogotsi, M.W. Barsoum, ACS Nano **6**, 1322-1331 (2012)

76. M. Naguib, V.N. Mochalin, M.W. Barsoum, Y. Gogotsi, Adv. Mater. **26**, 992-1005 (2014)
77. N.C. Osti, M. Naguib, A. Ostadhossein, Y. Xie, P.R.C. Kent, B. Dyatkin, G. Rother, W.T. Heller, A.C.T. van Duin, Y. Gogotsi, E. Mamontov, ACS Appl. Mater. Interfaces **8**, 8859-8863 (2016)
78. Y. Xie, M. Naguib, V.N. Mochalin, M.W. Barsoum, Y. Gogotsi, X. Yu, K.-W. Nam, X.-Q. Yang, A.I. Kolesnikov, P.R.C. Kent, J. Am. Chem. Soc. **136**, 6385-6394 (2014)
79. J.B. Mitchell, N.R. Geise, A.R. Paterson, N.C. Osti, Y. Sun, S. Fleischmann, R. Zhang, L.A. Madsen, M.F. Toney, D. Jiang, A.I. Kolesnikov, E. Mamontov, ACS Energy Lett. **4**, 2805-2812 (2019)
80. R.L. Sacci, M.L. Lehmann, S.O. Diallo, Y.Q. Cheng, L.L. Daemen, J.F. Browning, M. Doucet, N.J. Dudney, G.M. Veith, J. Phys. Chem. C **121**, 11083-11088 (2017)
81. W. Doster, M. Settles, Biochim. Biophys. Act. **1749**, 173-186 (2005)
82. A.P. Sokolov, J.H. Roh, E. Mamontov, V. Garcia Sakai, Chem. Phys. **345**, 212-218 (2008)
83. H. Frauenfelder, G. Chen, J. Berendsen, P.W. Fenimore, H. Jansson, B.H. McMahon, I.R. Stroe, J. Swenson, R.D. Young, Proc. Nat. Acad. Sci. **106**, 5129-5134 (2009)
84. S. Khodadadi, J.H. Roh, A. Kisliuk, E. Mamontov, M. Tyagi, S.A. Woodson, R.M. Briber, A.P. Sokolov, Biophys. J. **98**, 1321-1326 (2010)
85. E. Mamontov, X. Chu, Phys. Chem. Chem. Phys. **14**, 11573-11588 (2012)
86. S. Khodadadi, A.P. Sokolov, Soft Matter **11**, 4984-4998 (2015)
87. J.M. Parks, J.C. Smith, New Eng. J. Med. **382**, 2262-2264 (2020)
88. R.E. Amaro, J. Baudry, J. Chodera, O. Demir, J. A. McCammon, Y. Miao, J.C. Smith, Biophysical J. **114**, 2271-2278 (2018)
89. A. Acharya, R. Agarwal, M.B. Baker, J. Baudry, D. Bhowmik, S. Boehm, K.G. Byler, S.Y. Chen, L. Coates, C.J. Cooper, O. Demerdash, I. Daidone, J.D. Eblen, S. Ellingson, S. Forli, J. Glaser, J.C. Gumbart, J. Gunnels, O. Hernandez, S. Irle, D.W. Kneller, A. Kovalevsky, J. Larkin, T.J. Lawrence, S. LeGrand, S.-H. Liu, J.C. Mitchell, G. Park, J.M. Parks, A. Pavlova, L. Petridis, D. Poole, L. Pouchard, A. Ramanathan, D.M. Rogers, D. Santos-Martins, A. Scheinberg, A. Sedova, Y. Shen, J.C. Smith, M.D. Smith, C. Soto, A. Tsaris, M. Thavappiragasam, A.F. Tillack, J.V. Vermaas, V.Q. Vuong, J. Yin, S. Yoo, M. Zahran, L. Zanetti-Polzi, J. Chem. Inf. Model. **60**, 5832−5852 (2020)
90. M. Smith, J. C. Smith, ChemRxiv, Preprint. https://doi.org/10.26434/chemrxiv.11871402.v4
91. X. Hu, L. Hong, M.D. Smith, T. Neusius, X. Cheng, J.C. Smith, Nat. Phys. **12**, 171-174 (2016)
92. M. Trapp, M. Tehei, M. Trovaslet, F. Nachon, N. Martinez, M.M. Koza, M. Weik, P. Masson, J. Peters, J. R. Soc. Interface **11**, 20140372 (2014)
93. P. Tan, Y. Liang, Q. Xu, E. Mamontov, J. Li, X. Xing, L. Hong, Phys. Rev. Lett. **120**, 248101 (2018)
94. P. Tan, J. Huang, E. Mamontov, V. Garcia Sakai, F. Merzel, Z. Liu, Y. Ye, L. Hong, Phys. Chem. Chem. Phys. **22**, 18132-18140 (2020)
95. S. Li, P. Tan, J. Li, M. Tang, L. Hong, Phys. Rev. Res. **4**, L022003 (2022)
96. E. Persson, B. Halle, Proc. Natl. Acad. Sci. U. S. A. **105**, 6266-6271 (2008)
97. M.L. Martins, A.B. Dinitzen, E. Mamontov, S. Rudić, J.E.M. Pereira, R. Hartmann-Petersen, K.W. Herwig, N.H. Bordallo, Sci. Rep. **9**, 8704 (2019)
98. P. Ball, Proc. Natl. Acad. Sci. U. S. A. **114** 13327-13335 (2017)
99. J. Carvalo, S. Alves, M. Castro, C. Geraldes, J.A. Queiroz, C.P. Fonseca, C. Cruz, J. Pharmacol. Toxicol. Methods **95**, 70-78 (2019)
100. R. Ignazzi, W.P Gates, S.O. Diallo, D. Yu, F. Juranyi, F. Natali, H.N. Bordallo, J. Phys. Chem. C **121**, 23582–23591 (2017)
101. J. Kolosnjaj-Tabi, L. Gibot, I. Fourquaux, M. Golzio, M.-P. Rols, Advanced Drug Delivery Reviews **138**, 56-67 (2019)
102. S. Murdan, J. Control. Release **92**, 1–17 (2003)
103. M.L. Martins, J. Eckert, H. Jacobsen, E.C. dos Santos, R. Ignazzi, D.R. de Araujo, M.-C. Bellissent-Funel, F. Natali, M.M. Koza, A. Matic, E.de Paula, H.N. Bordallo, Int. J. Pharm. **524**, 397–406 (2017)
104. M.L. Martins, R. Ignazzi, J. Eckert, B. Watts, R. Kaneno, W.F. Zambuzzi, L. Daemen, M.J. Saeki, H.N. Bordallo, Sci. Rep. **6**, 22478 (2016)
105. M. Salvador-Castell, M. Golub, N. Martinez, J. Ollivier, J. Peters, P. Oger, Soft Matter **15**, 8381-8391 (2019)
106. M. Golub, B. Lehofer, N. Martinez, J. Ollivier, J. Kohlbrecher, R. Prassl, J. Peters, Sci. Rep. **7**, 46034 (2017)
107. A. Cisse, A.L. Schachner-Nedherer, M. Appel, C. Beck, J. Ollivier, G. Leitinger, R. Prassl, K. Kornmueller, J. Peters, J. Phys. Chem. Lett. **12**, 12402-12410 (2021)
108. E. Mamontov, Y. Cheng, L.L. Daemen, J.K. Keum, A.I. Kolesnikov, D. Pajerowski, A. Podlesnyak, A.J. Ramirez-Cuesta, M.R. Ryder, M.B. Stone, ACS Omega **5**, 21231-21140 (2020)
109. E. Mamontov, Y. Cheng, L.L. Daemen, A.I. Kolesnikov, A.J. Ramirez-Cuesta, M.R. Ryder, M.B. Stone, J. Phys. Chem. Lett. **11**, 10256-10261 (2020)